Particle & Particle Systems Characterization
www.particle-journal.com

Anisotropic Thermal Processing of Polymer Nanocomposites via the Photothermal Effect of Gold Nanorods

*Somsubhra Maity, Krystian A. Kozek, Wei-Chen Wu, Joseph B. Tracy, Jason R. Bochinski, and Laura I. Clarke**

By embedding metal nanoparticles within polymeric materials, selective thermal polymer processing can be accomplished via irradiation with light resonant with the nanoparticle surface plasmon resonance due to the photothermal effect of the nanoparticles which efficiently transforms light into heat. The wavelength and polarization sensitivity of photothermal heating from embedded gold nanorods is used to selectively process a collection of polymeric nanofibers, completely melting those fibers lying along a chosen direction while leaving the remaining material largely unheated and unaffected. Fluorescence-based temperature and viscosity sensing was employed to confirm the presence of heating and melting in selected fibers and its absence in counter-aligned fibers. Such tunable specificity in processing a subset of a sample, while the remainder is unchanged, cannot easily be achieved through conventional heating techniques.

1. Introduction

In this work, the photothermal effect of gold nanorods (GNRs) is used to selectively process a collection of polymeric nanofibers, for example, completely melting those fibers lying along a chosen direction while leaving the remaining material largely unheated and unaffected. While melting is utilized as a proof-of-principle to demonstrate this effect, such capability could be usefully utilized for any level of thermal processing. This ability to select only a subset of the sample, heat it dramatically and thus transform it in situ, is due to the innate specificity of the plasmon-mediated photothermal effect of metal nanoparticles embedded within the nanofibers. In particular, heating occurs only where 1) GNRs are present and 2) the wavelength *and polarization* of the light irradiation match the GNRs' surface plasmon. Although most studies of the photothermal properties of metal nanoparticles have been performed in solution, this specificity is highlighted in solid environments where the particle placement can be non-uniform and particle orientation can be controlled, the latter point being the focus of this work. Thus the specificity of the photothermal effect provides the ability to create and modify nanostructured materials by design, for instance driving phase-transitions,[1,2] cross-linking, or chemical reactions, or manipulating crystallinity in situ solely within specific subsets of a material, even if such subsets spatially overlap. One example of the unique potential power of the photothermal processing scheme, where the heat is generated from within the material, is uniformly irradiating an entire homogeneous sample, but using the polarization of the light to selectively "break the symmetry" and only couple heat into the sample along a single direction, even though GNRs are equally present in all fibers. Here, electron microscopy is used to monitor changes in the morphology of nanofibrous materials under photothermal heating; in addition, a fluorescence-based thermometer measures the average temperature in the sample interior, and fluorescence polarization anisotropy is used to confirm melting. By selective placement of the temperature- and viscosity-sensing fluorophores, the absence of heating in sample regions with GNRs not aligned with the light field linear polarization direction is confirmed.

In the photothermal process, visible light is absorbed by metal nanoparticles due to a resonance with the collective electron oscillation referred to as the surface plasmon.[3] Because of the absence or weakness of radiative relaxation mechanisms, the conversion of optical energy into heat via non-radiative electron relaxation[4,5] is the dominant process, resulting in strong photothermal properties. As previously demonstrated, [1,2] polymer nanofibers and films containing even low concentrations of spherical gold nanoparticles can be heated to a few hundred °C by irradiation with relatively low-intensity resonant light. Amongst the different types of metal nanostructures, anisotropic gold nanorods (GNRs) are a useful choice for photothermal applications[6,7] due to their optical properties, which include a widely-tunable longitudinal surface plasmon

S. Maity, J. R. Bochinski, L. I. Clarke
Department of Physics
NC State University
2401 Stinson Drive,Box 8202
Raleigh, NC, 27695-8202, USA
E-mail: laura_clarke@ncsu.edu
K. A. Kozek, W.-C. Wu, J. B. Tracy
Department of Materials Science and Engineering
NC State University
Raleigh, NC, 27695, USA

DOI: 10.1002/ppsc.201200084

resonance (LSPR) along the GNR long axis in addition to a less easily varied, weakly size-dependent transverse surface plasmon resonance (TSPR). Since the LSPR can be adjusted from the visible to the near infrared spectral region by altering the nanoparticle aspect ratio, GNRs have been widely used in biological systems, as infrared wavelengths have increased tissue penetration.[8–10] A more subtle advantage of GNRs is their additional polarization sensitivity: light is only absorbed by the LSPR (TSPR) if the linear polarization direction overlaps the long (short) axis of the nanorod. While a few earlier studies have utilized the polarization dependence of GNRs,[11,12] to our knowledge, its efficacy in photothermal applications[13] has not been previously explored.

2. Results and Discussion

2.1. Nanoscale and Macroscale Alignment of GNRs

Several schemes have been reported that incorporate GNRs within or atop of an ordered solid material environment:[14–23] we have employed GNRs embedded in polymer nanofibers[24–26] fabricated by electrospinning[27,28] from a polymer solution containing GNRs. This technique is particularly useful because although the GNRs in solution are randomly oriented, electrostatic and viscoelastic forces present during fiber formation effectively align GNRs along the resultant nanofiber axis,[24] thus correlating the orientation of the fiber and that of the GNRs. Other groups have also recently used nanoparticles when electrospinning to assemble nanostructures.[29,30]

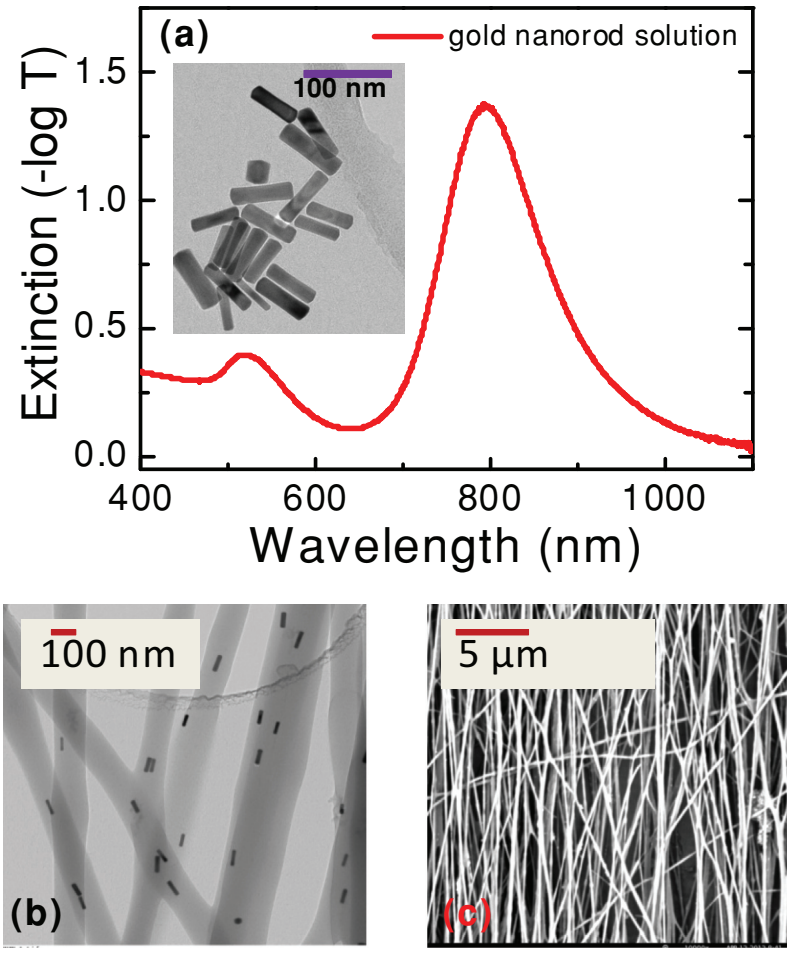

Figure 1. (a) The extinction spectrum of the 0.005% volume fraction CTAB-capped GNR solution in a CTAB-water solution, with a transmission electron micrograph (TEM) image (inset). (b) TEM image depicting the alignment of GNRs in randomly-oriented nanofibers. (c) Scanning electron micrograph (SEM) of vertically-aligned nanofibers depicts an additional level of control over GNR/fiber orientation.

The GNRs employed in this study were fabricated by a seed-mediated growth method (unpublished) that gives comparable results to a commonly used approach[31] and resulted in hexadecyltrimethylammonium bromide (CTAB)-capped GNRs having an average aspect ratio of ~4.0 ± 1.8 (length = 68 ± 13 nm; width = 17 ± 7 nm; **Figure 1**a inset) with a small fraction of spherical nanoparticles (~10%). The extinction spectrum of the GNR solution was measured in a commercial ultraviolet-visible absorption spectrometer. The peak extinction in solution due to the LSPR was at ~800 nm and that of the TSPR at ~520 nm, as shown in Figure 1a. The spherical nanoparticles present also possess a surface plasmon resonance (SPR) that overlaps the spectral region of the TSPR of the GNRs. Poly(ethylene oxide) (PEO) was used as the matrix to host the GNRs. The polymer nanocomposite fibers were fabricated using traditional needle-electrospinning where further details of the electrospinning procedure are provided in the Materials and Methods section. The solid polymeric nanofibers obtained contain 2.5 wt% (0.15% volume fraction) GNRs. The randomly-oriented nanofibrous mat (Figure 1b) was comprised of nanofibers with diameters of 227 ± 32 nm. Figure 1b reveals the orientation of the GNRs within the randomly-arranged polymer nanofibers, as shown by a characteristic transmission electron microscopy (TEM) image. The GNRs are almost perfectly aligned along the direction of the axis of the nanofibers with an average deviation angle $\phi = 2.85 \pm 0.68°$.

The macroscale alignment of the GNRs to the nanofiber axis can also be demonstrated by fabricating mats comprised of oriented fibers. The same basic electrospinning arrangement was utilized, but instead of a flat collector, a grounded, rotating cylindrical mandrel was used to gather nanofibers oriented perpendicular to the mandrel axis of rotation, resulting in an average fiber deviation angle of 7.82 ± 1.92°, as shown in a scanning electron microscope (SEM) image (Figure 1c). This fabrication setup is similar to others previously reported.[24,32,33] In such uniaxially fiber-aligned mat samples (nanofiber diameter 165 ± 27 nm), the extinction spectrum will depend on the angle between the input light linear polarization and the fiber alignment directions due to the orientation of the nanofibers, and subsequently the GNRs (**Figure 2**, inset).[24]

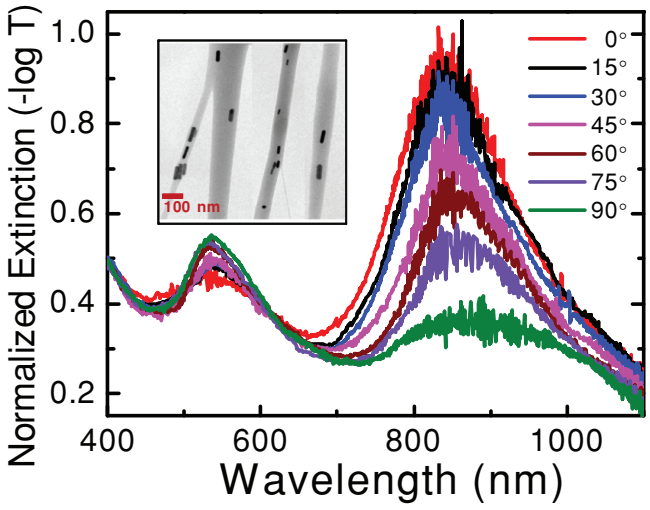

Figure 2. Normalized extinction spectra of uniaxially-aligned PEO:GNR nanofibers fabricated on a transparent substrate with varying relative angles of the incident light linear polarization orientation from 0° (parallel) to 90° (perpendicular) relative to the fiber alignment direction. The feature at ~535 nm has contributions from both the TSPR of the GNRs and the SPR of the small population of spherical nanoparticles in the sample; the spherical nanoparticles display no polarization sensitivity. The peak at ~850 nm (solely due to the LSPR of the GNRs) decreases as the relative angle changes from parallel to perpendicular. A background subtraction equal to the extinction of a similarly-thick, PEO-only oriented fibers has been applied to each angle. The data has been normalized to the peak of the LSPR of the GNRs at 0°. Inset: TEM image of vertically aligned PEO:GNR nanofibers.

Figure 2 shows extinction spectra where the input light is linearly-polarized at varying angles from 0–90° relative to the fiber/GNR alignment axis. As seen previously in Figure 1a, the smaller extinction feature at ~535 nm has contributions from both the TSPR of the GNRs and the SPR of the spherical nanoparticles whereas the large extinction peak at ~850 nm results only from the LSPR of the GNRs. Both peaks are red-shifted in wavelength from their values in solution (Figure 1a) due to the different dielectric environment of the polymer matrix.[34] Because the nanorods are uniformly oriented within the polymer matrix, there now exists a polarization as well as a spectral dependence of the GNRs' interaction with the incident light field; that is, both the wavelength of the light and its polarization direction must be matched to the GNRs alignment in order to effectively couple to the nanoparticle. Such directional selectivity with polarized light is not possible when nanoparticles are homogeneously organized in media such as the previous solution case, or if the particles lack anisotropic shapes (e.g., nanospheres). Thus, when the incident light linear polarization direction is parallel to the long axis of the GNRs (i.e., 0°), the LSPR peak at ~850 nm is maximized and the extinction feature at ~535 nm is minimized. In the parallel orientation, the ~535 nm peak has contributions from the polarization-independent SPR of the small quantity of spherical nanoparticles present, as well as the TSPR of imperfectly aligned GNRs. As the relative angle between the GNR axis and polarization direction is increased, the LSPR peak decreases and in a correlated fashion, the TSPR extinction feature grows until at 90°, the ~850 nm peak is minimized and the ~535 nm peak is fully enhanced.

An analogous experiment was performed by leaving the input linear polarization unchanged and instead physically rotating the sample, demonstrating the same results as in Figure **2**. In contrast, an aligned PEO nanofibrous mat comprised of only spherical gold nanoparticles (i.e., no GNRs) displayed no such angle dependence (Supporting Information). Thus, these extinction experiments demonstrate explicitly that the light at ~850 nm is not absorbed by the GNRs when its linear polarization direction is perpendicular to the GNRs' long axis; this elegant control over the light field–nanoparticle interaction can subsequently be used to generate spatially selective heating via the photothermal effect within polymer nanocomposite samples.

2.2. Fluorescence-Based Temperature-Sensing and Photothermal Heating

In order to quantify the temperatures reached within fibers aligned or perpendicularly-oriented to the irradiation polarization, a fluorescence-based temperature-sensing technique was employed to monitor the average change in temperature of the nanocomposite in situ. A dilute concentration of a fluorescent molecule, perylene, was also incorporated into the nanofibers (i.e., added to the PEO-GNR solution prior to electrospinning). The randomly-distributed fluorophores exhibit several vibrational absorption peaks within the electronic $S_0 - S_1$ transition in the wavelength range between 365 – 435 nm; the resulting fluorescence features range from 435 – 550 nm. The ratio between two specific emission spectral features – the trough occurring at ~465 nm and the peak at ~ 480 nm – is approximately linear with temperature. By comparison with a calibration curve generated by conventional heating of a composite sample, the fluorescence ratio can be used as a quantitative internal thermometer[1,35] during photothermal heating. Therefore, in addition to the heating irradiation light at 808 nm, a second probing laser beam at 405 nm was spatially-overlapped with the first and utilized to selectively excite the perylene molecules; the resultant emission was analyzed to determine the average sample temperature. Additional details for the optical measurements are presented in previous work[1] and in the Experimental Section. The use of an emission ratio makes this method robust to fluctuations in excitation laser intensity, local variations in dye concentration, and temperature-induced shape changes of the overall emission band profile.

As an example of the utility of this technique, the internal average temperature within uniaxially vertically-aligned nanofibers (**Figure 3**a), containing 0.02% volume fraction of perylene and 0.15% volume fraction of GNRs, was observed as a function of time during irradiation with vertical linear polarization (0.1 W/cm^2 at 808 nm). The average sample temperature increases over ~10 minutes until stabilizing at 66.5 ± 1.2 °C (solid red circles, Figure 3d), approximately the melting point of poly(ethylene oxide) (T_m = ~66 °C). SEM images (Figure 3b) confirm that the nanofibers experience a material phase-change under this illumination. In contrast, irradiating such a sample with identical light which was horizontally linearly polarized showed no increase in temperature (open blue squares,

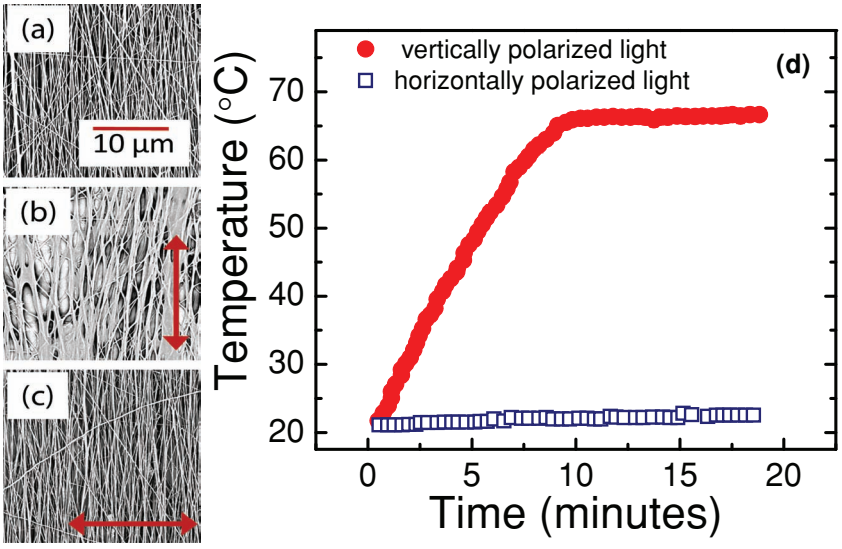

Figure 3. SEM images of (a) as-fabricated, vertically-aligned nanofibrous mat. (b) The same mat after treatment with vertically polarized 0.1 W/cm^2 808 nm light for 20 minutes results in extensive fiber melting. (c) The same mat exposed to the same intensity, duration, and wavelength of light but horizontally polarized . The GNRs are perpendicularly-oriented to the incident light polarization direction and thus, do not produce heat. Temperature plots of the two cases: (d) With vertical linear polarization (solid red circles), the mats are heated to approximately the melting temperature of the polymer (~66 °C); in contrast, when horizontal linear polarization is used (open blue squares), virtually no change in the average temperature of the fibers is observed. All SEM images are taken at the same magnification. Red arrows indicated the polarization direction of the incident light.

Figure 3d), consistent with the electron microscopy images that revealed no alteration in the mat morphology (Figure 3c). The incident light is simply not absorbed because there are essentially no particles correctly oriented with respect to the light polarization (horizontal) and therefore, no heating can occur. Thus, this measurement demonstrates the specificity of the polarization-controlled heating by the GNRs.

2.3. Polarization-Selective Photothermal Treatment

To further demonstrate GNR polarization-dependent photothermal heating, a four-layer cross-hatch patterned mat was fabricated, in which alternating nanofiber layers were horizontally and vertically aligned (accomplished by briefly interrupting the electrospinning process and reorienting the mat on the collector mandrel). **Figure 4** shows the SEM images of the cross-hatched nanofibers as-spun (terminating in either vertical (Figure 4a) or horizontal (Figure 4b) layers). Irradiation of the entire sample with linear, vertically polarized 808 nm light (intensity 0.1 W/cm^2, for 20 minutes) resulted in heating and melting of the layers of vertically-aligned fibers while the layers of horizontal fibers remained intact (Figure 4c,e, and h), regardless of which oriented layer was top-most. Similarly, utilizing the same irradiation intensity and time interval but with horizontal linear light polarization resulted in completely melting of solely the horizontal fibers, leaving the layers of vertical fibers undamaged (Figure 4d,f, and g). The light is only absorbed by the subset of fibers that contains GNRs with an orientation that matches the light polarization. Counter-aligned (long axis perpendicular to the polarization direction) GNRs absorb no light and thus no heating occurs in counter-aligned fibers. Thus, asymmetric thermal processing can be achieved under uniform light irradiation (and with GNRs present in all fibers) by utilizing the inherent polarization sensitivity of the anisotropic embedded nanoparticles.

Perylene molecules were incorporated within either horizontal or vertical fibers in the cross-hatched mat samples in order to track the temperatures of the different layers, which are anticipated to vary significantly. Figure 4i shows the independent temperature curves for either the vertical or horizontal layers for a cross-hatched patterned mat experiencing vertically-polarized irradiation. As expected, the vertical fibers (solid purple squares, Figure 4i) warm over a period of ~10 minutes to an average steady-state temperature of 66.4 ± 1.1 °C, which is consistent with the previous experiment on the uniaxially-aligned mats (Figure 3b, d) and the overt melting observed when the orientation of the nanofiber layer and linear polarization direction are matched in Figure 4. There is no direct photothermal heating due to the GNRs within the horizontal fibers because of the mismatch with the polarization of the incident light. The horizontal fibers however will slowly heat due to thermal conduction because they are in physical contact with the vertical fibers (open blue circles, Figure 4i). Nevertheless, even after 30 minutes of irradiation, the horizontal fibers have reached a steady-state temperature, which is well below the polymer melting point (T = ~50 °C), consistent with their intact structure, as shown in the SEM images in Figure 4.

2.4. Fluorescence Anisotropy to Detect Phase Transition

The thermal environment within the polymer matrix can be confirmed by utilizing the dilute embedded perylene molecules in a different manner: to measure fluorescence anisotropy which quantifies the ability of a fluorescent molecule to reorient and hence, is sensitive to the decrease in local viscosity when melting occurs. A light source that is linearly-polarized (in this case, a violet laser at 405 nm that selectively interacts with the perylene) preferentially excites fluorophores oriented such that their absorption transition moment is primarily aligned parallel to the incident polarization vector. Thus, if the excited molecules cannot reorient in the few ns excited state lifetime before emission (as the case within a solid material matrix), the subsequently observed emission will also be polarized in the same direction as the excitation source (for the case where the emission transition dipole is oriented along a similar direction as the absorption dipole). However, if during the excited state lifetime, the fluorescing molecule rotates, then its subsequent emission will reflect this depolarization. The extent of polarization of the

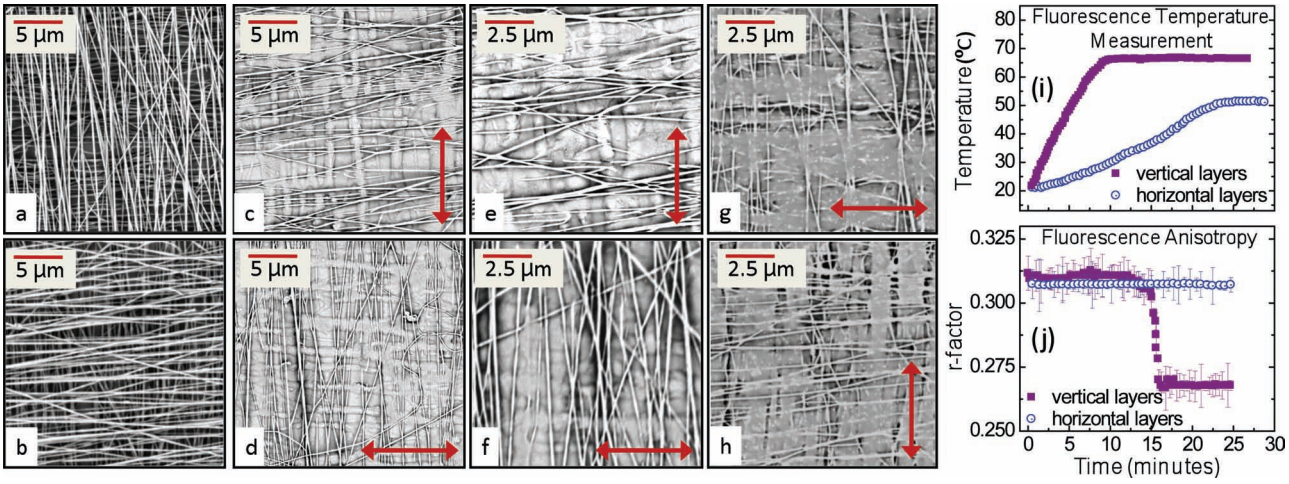

Figure 4. As-fabricated PEO:GNR cross-hatched nanofibrous mats terminating in (a) vertical or (b) horizontal layers, respectively. When (a) is treated with vertically-polarized red laser: (c), (e) only the vertical layer melts as shown at two different magnifications. When (b) is treated with horizontally polarized light: (d), (f) only the horizontal layers melt as shown at two different magnifications. (g) and (h) depict cases when the top layers and the incident light polarization do not match and remain intact while the underlying matched layers are heated, melt, and wet the top layers. The red arrows depict the polarization direction of the incident light. Thus samples shown in each row all began as the left-most (as-spun) image. The observed changes are due to irradiation with light of different polarization. (i) The average temperature versus time while heating, measured for the vertical (solid purple squares) and horizontal (open blue circles) layers when only the vertical layer is photothermally-excited. (j) The change in fluorescence anisotropy of the vertical (solid purple squares) and horizontal (open blue circles) layers under the same heating conditions. The laser intensity is fixed at 0.1 W/cm^2.

emission is described by the anisotropy parameter *r-factor*[36,37] given as:

$$r = \frac{I_{||} - I_{\perp}}{I_{||} + 2I_{\perp}}$$

where $I_{||}$ and $I_{\perp}$ are the fluorescence intensity measurements parallel and perpendicular to the incident polarizations, respectively. The *r-factor* is maximized when the molecule cannot reorient, and decays toward a value of zero for cases where facile molecule reorientation can occur before emission (e.g., low viscosity liquids). In a liquid regime (such as molten polymer), *r* will have a lower value than in a solid and becomes smaller with increasing temperature, as the viscosity of the environment decreases. Perylene has a published anisotropy value of $r = 0.32 \pm 0.018$ when embedded within solid media.[38–40]

Fluorescence anisotropy experiments were carried out within a commercial spectrofluorometer with a separate external laser for in situ photothermal heating, or utilizing a homemade apparatus that allowed for either photothermal heating or conventional heating of the sample using a hot plate. The measured perylene anisotropy *r-factor* in room-temperature PEO:GNR nanofibers was 0.31 ± 0.015, overlapping both the literature value and the *r-factor* determined from a bulk sample cast from solution (0.322 ± 0.012). Heating the solution-cast polymer sample to 80 °C on a hot plate (with sufficient time between heating steps to allow thermal equilibration) showed no change until 65 °C (during the solid phase regime) and then a smooth reduction in anisotropy above the melting point to a value of 0.243 ± 0.011 at 80 °C (Supporting Information). When a cross-hatched mat, where perylene was incorporated only within the vertical fibers, was irradiated with vertically-polarized 808 nm light, the anisotropy began decreasing slowly at the 10 minute mark and then dropped suddenly to 0.265 ± 0.08 at 15 minutes, indicating that fiber melting had occurred (filled purple squares, Figure 4j) consistent with the time-scale of the temperature measurement (Figure 4i). This*r-factor* value indicates that the vertical fibers are now in an environment of molten polymer at a temperature of ~70 °C, which is fully consistent with both the ratio temperature measurement and the SEM images. In contrast, ther*-factor* for perylene solely within the horizontal fibers is constant due to the absence of any melting (open green circles, Figure 4j). Hence, the independent fluorescence measurements of temperature and anisotropy both confirm the SEM images in demonstrating the selective nature of photothermal heating using GNRs. By placing the sensing perylene fluorophores in different nanofiber layers, the asymmetric heating of the mat samples can be elegantly demonstrated and the different average local temperatures quantified.

2.5. Mechanism of Anisotropic Melting of Polymer Fibers

To more precisely elucidate the manner in which the vertical fibers relax, aggregate, then melt and flow through the horizontal layer when experiencing the temperature/time curve in Figure 4i, a time-sequence electron-microscopy study was conducted for cross-hatched patterned mats irradiated with vertically linearly polarized light for 5, 10, 12, 14, and 16 minutes (**Figure 5**). As expected from the measured heating curve, little change is observed until approximately 10 minutes, when the polymer-matrix melting temperature is reached and the vertically-oriented fibers containing GNRs begin to soften, relax, and thus, aggregate. Due to this inhomogeneous fiber fusing, more of the background (i.e., the unheated horizontally-aligned

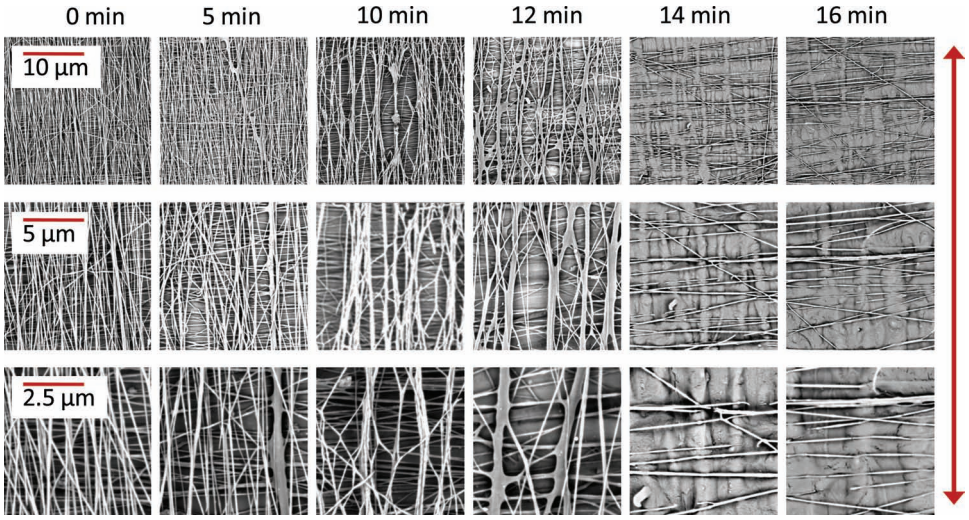

Figure 5. Time sequence of photothermal treatment of cross-hatched mats with vertically polarized light, at different magnifications. There are few observable changes in the fibers until at 10 minutes, the fibers begin to soften, relax, and aggregate together. By 12 minutes, the fiber bundles in the top layer start fusing together. Melting and flow of resulting polymer leads to the formation of distinct anisotropic melt patterns, as seen at 14 and 16 minutes. Images in the same column were treated for identical duration, while images within the same row have the same magnification. The laser intensity is fixed at 0.1 W/cm^2.

PEO:GNR layers) is exposed. At 12 minutes, the vertical fiber bundles in the first layer have fused; by 16 minutes, almost all the vertical fibers have melted and only the top-most fibers in the horizontal layer are visible, protruding from the film formed by the melted vertical fibers.

As a further example of this selective thermal processing approach, randomly-oriented PEO:GNR mats were irradiated with 808 nm light (0.25 W/cm^2) having identical intensities but different polarizations (**Figure 6**). When using linearly polarized light, the irradiation will couple predominantly to the GNRs (and thus fibers) oriented parallel to the polarization direction and is expected leave those fibers aligned primarily perpendicular to this direction largely unaffected. As shown in Figure **6**b after 10 minutes of treatment, fibers that were predominantly oriented along the vertical direction were well-matched to the linear light polarization and experienced the strongest photothermal heating, aggregating to the extent possible given the contacts with the non-heated fibers and melting, thereby inducing anisotropy within an originally isotropic, random sample (Figure **6**a). Fibers oriented at other angles but with some component along the vertical direction also experienced photothermal heating, although to a lesser extent. In contrast, utilizing circularly polarized light will photothermally-couple equally to every GNR in the sample (i.e., to all fiber or nanorod orientations) and therefore, is expected to uniformly heat the sample. Thus, nanofibers irradiated with circularly polarized light at the same intensity do not experience selective thermal treatment and demonstrate homogeneous melting (Figure **6**c). **Figure 7**a quantifies the asymmetry created by the selective thermal processing: the as-spun fibers are relatively narrow (267 ± 50 nm as indicated by the horizontal dashed line) and have no size-dependent orientation (solid black squares). After

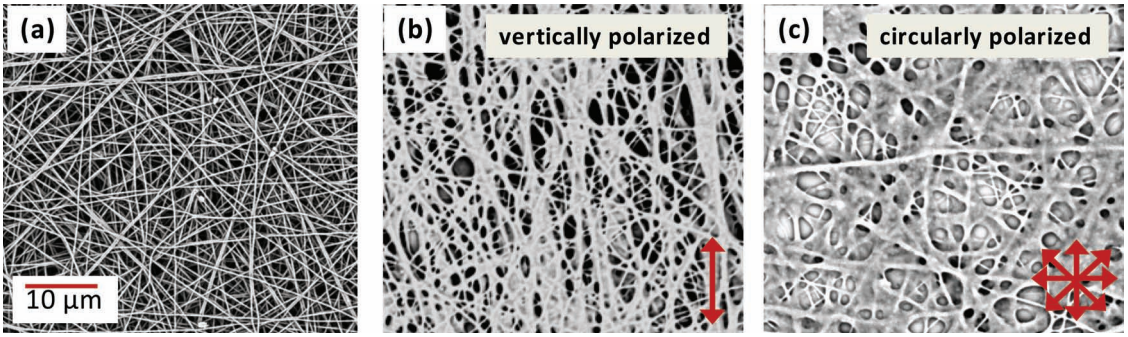

Figure 6. SEM images of (a) as-spun randomly-oriented nanofibers, depicting an isotropic distribution of fibers. When such mats are treated with (b) vertically polarized 0.25 W/cm^2 red light for 10 minutes, only the fibers with a component along the vertical direction are heated, leading to melting and fusion of these fibers. As a result, an anisotropic melt pattern is created from the original random mat. In comparison, when a similar random mat is treated with the same intensity and duration of (c) circularly polarized light, it results in melting of all fibers without any preferred direction. All images are acquired at the same magnification and the red arrows indicate the polarization direction of the incident light.

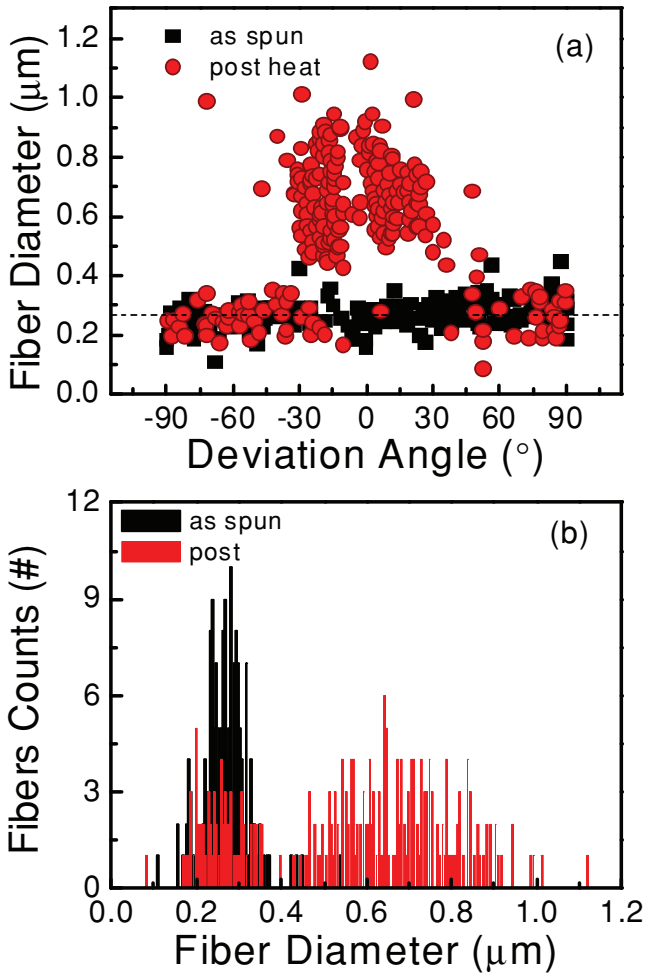

Figure 7. (a) The asymmetry produced after directional heating can be quantified by analyzing fiber diameters as a function of angular orientation before and after thermal treatment. (b) Change in the distribution of fiber diameters via the photothermal processing. The as-fabricated mat has smaller diameter fibers (267 ± 50 nm) and a narrower distribution (black columns); after photothermal treatment, a new population of larger diameter fibers (red columns) has been formed.

10 minutes of photothermal treatment (solid red circles), fibers aligned along or near to (< ±~30°) the linear polarization direction experienced the most heating undergoing relaxation, aggregation, and fusion to form larger diameter structures, while those at greater angles remain largely unaffected. Figure 7b quantitatively displays the effects of photothermal treatment on fiber diameters: the as-fabricated mat (black columns) has predominantly smaller diameter fibers with a relatively narrow distribution (267 ± 50 nm); post-thermal processing, a new population of fibers having larger diameters (red columns) is generated by the relaxation, agglomeration, and fusion of the GNR-heated fibers. SEM images of the time sequence at 5 and 7 minutes of irradiation with vertically polarized incident light are displayed in **Figure 8**, where the stages of fiber relaxation, aggregation, and finally melting are clearly discerned. Hence, in the case of a random-oriented nanofibrous mat, such selective polarized photothermal treatment via the GNRs can produce anisotropy within an initially isotropic environment.

3. Conclusions

In summary, this work highlights the useful specificity of the photothermal effect of anisotropic nanoparticles for selective, in situ processing of materials. In particular, use of photothermal heating by GNRs enables selection of a subset of the sample and complete thermal processing of that subset (e.g., melting, cross-linking, driving of a chemical reaction, or curing) while leaving the remainder unchanged. Importantly, the selected subset need not be spatially separate from the remainder of the sample and the entire sample is irradiated. As demonstrated here, fibers were fully melted while immediately neighboring perpendicular fibers were unchanged. Isolation between components selected for processing and the non-selected portions is enhanced because heating occurs *within* the selected fibers - with the warmest temperatures occurring at the embedded GNRs rather than at the fiber surface, minimizing heating of the non-selected sample components. Finally, such an approach only requires irradiation with relatively weak light and the surface plasmon resonance can be tuned (by altering the particle aspect ratio) to minimize non-specific interactions with the surrounding environment. Thus, heat can be selectively placed at the 100 nm scale, even for a material in-service where surrounding parts are heat sensitive or within a biological environment. With the combined use of a highly sensitive, fluorescence-based temperature sensing technique and fluorescence anisotropy to measure viscosity, the material response can also be monitored in real time. Such tunable specificity in processing a subset of a sample while the remainder is unchanged cannot easily be achieved through conventional heating techniques.

4. Experimental Section

Fabrication and characterization of GNR-doped polymer nanocomposite: Poly(ethylene oxide) (PEO) (Sigma Aldrich; molecular weight 900, 000 g/mol) solutions in de-ionized water were mixed with the aqueous GNR solution and perylene powder to form a 4 wt% PEO solution, which ultimately resulted in a 2.5 wt% (0.15% volume fraction) of GNRs and 0.09 wt% (0.02% volume fraction) of perylene (Sigma Aldrich) in the solid nanofibrous sample after electrospinning. The final solution was magnetically stirred for 8–10 hours at room temperature before electrospinning.

The perylene:GNR:PEO solution was electrospun in a traditional needle electrospinning setup, using a feed rate of 6 μL/minute and an applied positive polarity voltage of 15 kV. The syringe had a volume of 12 mL and the stainless steel 20 gauge needle was 10 cm long. The electrospinning apparatus consisted of a programmable syringe pump (New Era Pump Systems, Model NE 500) and a high voltage power supply (Glassman High Voltage, Model No. FC60R2) electrically attached to the conducting needle and the collector as the return path, respectively. The needle-to-collector working distance was 20 cm. The resultant randomly oriented nanofibers were gathered on aluminum foil placed on the grounded collector, and mat samples were photothermally- or traditionally-treated without further processing. To obtain unidirectionally-aligned nanofibrous samples, a custom-made, grounded, rotating (3500 rpm) cylindrical mandrel (covered with aluminum foil) was substituted for the flat collector and the working distance was reduced to 10 cm. The mandrel was 38.1 cm long, with a diameter of 7.62 cm. Cross-hatched patterned mats were obtained by electrospinning for a brief period, pausing and reorienting the foil by 90° on the mandrel, and then repeating the process for each layer. For

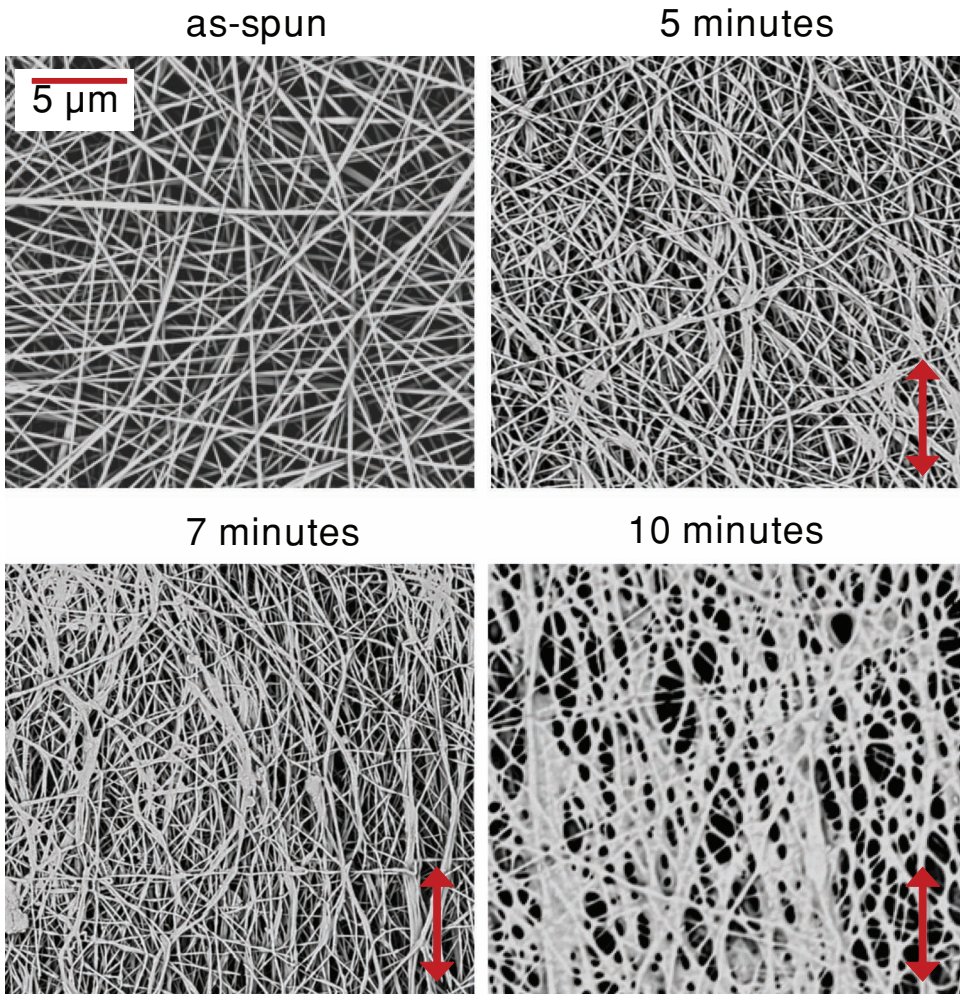

Figure 8. SEM images of a PEO:GNR randomly-oriented nanofibrous mat, initially as-spun, and after 5, 7, and 10 minutes of treatment with vertically-polarized, 0.25 W/cm^2 808 nm light. After 5 minutes, the nanofibers show significant relaxation and curling, and some signs of fiber fusion. This fiber fusion and aggregation becomes more pronounced after 7 minutes, with a predominant orientation parallel to the laser polarization (i.e., vertical). After 10 minutes, the aggregated fibers display widespread melting, thus creating a pseudo-vertical pattern in the mat. All images were taken at the same magnification. The red arrow indicates the polarization direction of the excitation light.

experiments with selective placement of perylene, the spinning solution was also switched (otherwise identical solutions with or without the perylene) between each layer deposition. Aligned mats for absorbance spectroscopy and the fluorescence anisotropy experiments were collected on a flexible, transparent plastic sheet wrapped around the mandrel.

The resultant fibers were imaged using a scanning electron microscope (SEM) (FEI Phenom-World BV); fiber size and porosity analysis[41–44] utilized ImageJ software. SEM images acquired at 20 000× magnification were used to calculate the average fiber diameter and distribution, resulting in 227 ± 32 nm and 165 ± 27 nm for random and aligned samples, respectively. The mat porosity was calculated as the relative number of marked and unmarked pixels (solid material and void space) in the topmost mat layer; the porosity of the random mats was ~70%. The sample thickness was measured by an alpha step profilometer (Veeco Dektak Model 150) and found to be 5–7 μm for both random and aligned mats. Our previous work[1] demonstrated light penetration, independent of wavelength over the visible spectral range, at similar intensities as used in this work, with samples of comparable thicknesses. Dispersion of the GNR within the nanofibrous mats was confirmed from transmission electron microscopy (TEM) images which were obtained using a Hitachi HF2000 or a JEOL 2000FX transmission electron microscope.

The extinction measurements were carried out using an ultraviolet-visible absorption spectrometer (CARY 50 Scan). When determining the extinction spectrum of the GNRs in solution phase, a concentrated GNR solution was diluted to 0.005% volume fraction using a CTAB-water (0.034 g/mL) solution. For measuring the extinction of GNRs within nanofibers and studying their polarization sensitivity, experiments were performed on aligned fibers fabricated (as described above) on a transparent substrate; that is, instead of using aluminum foil for collecting the nanofibers on the mandrel, a flexible plastic transparency was utilized. For the first set of absorption experiments, the sample was kept stationary; a linear polarizer and appropriately aligned $\lambda/4$ plate in the beam path created circularly polarized light before a final linear polarizer inserted prior to the sample was rotated from 0°–90° in increments of 15°. For the second series of measurements, the rotatable linear polarizer was fixed and instead, the sample itself was rotated from 0°–90° in increments of 15° (Supporting Information, Figure S1a). An

identical experiment was performed with unidirectionally-aligned fibers doped solely with spherical gold nanoparticles to demonstrate the angle-independent extinction of the nanospheres (Figure S1b).

Non-contact temperature-sensing using fluorescent probes: A violet 405 nm continuous-wave diode laser (operated at ~5 mW power) expanded to a collimated ~5 mm diameter spot size, flywheel-chopped at 2 kHz, was used to excite the perylene molecules in the PEO:GNR composite samples. A 50:50 beamsplitter served to front illuminate the sample while the other portion, sampled by a photodiode coupled to a lock-in amplifier, monitored fluctuations in laser amplitude. A set of 50 mm diameter biconvex and 50 mm cylindrical lenses (both having focal lengths of 6 cm) was arranged serially to gather and image the fluorescence onto the input slit of a double-grating scanning monochromator (SPEX 1680B). The scattered components of the incident violet and red lasers were blocked by a 435 nm dielectric low pass interference filter (Omega Optical) and a short pass 532 nm dichroic beamsplitter (CVI), leaving an open spectral window over the perylene emission range. The output signal from the monochromator was detected by a side-on photomultiplier tube (PMT) detector (Hamamatsu 931B) operated at ~800 V. The spectral resolution of the measurement was ~1 nm. The amplified PMT output was photon-counted (Stanford Research Systems SR400), with a corresponding background subtraction from equal counting times when the violet laser was blocked. No attempt was made to further spectrally correct the observed fluorescence for the interference filter, monochromator grating, or PMT photocathode response.

Previous work[1,35] has identified a quasi-linear relationship between particular spectral fluorescence features of perylene and the sample temperature. The full emission spectrum of perylene and its temperature dependence are shown in Supporting Information. The overall perylene fluorescence intensity decreases as the average sample temperature increases (Figure S2a) in such a manner that the particular trough-to-peak ratio (trough (465 nm) and peak (479 nm)) increases with temperature (Figure S2b). For temperature calibration, the sample stage was externally-controlled (LakeShore Model 331) with a resistive heater and the temperature varied from room temperature (~20 °C) to 80 °C (above the melting point of PEO) in order to generate a calibration curve. The overall experiment was computer-controlled by a user-written program (LabView) to iteratively tune the monochromator, control the stage temperature, and sequentially measure and record both the fluorescence and laser amplitudes.

Photothermal heating and in situ temperature sensing: The output of a red 808 nm, 800 mW continuous-wave diode laser was used for the photothermal experiments. The laser beams were expanded using positive lenses and spatially aligned such that the spot size of the red beam completely overlapped the smaller-sized probe violet laser beam for all measurements. The unfiltered red laser beam after passing through all beam-shaping and directing optics was initially determined to be elliptically polarized (5:1 in the vertical direction) at the sample. A combination of linear polarizers, quarter-wave plates, and half-wave plates (Melles Griot, Thor Labs) were inserted to obtain circularly-polarized, or linearly-polarized (either horizontally or vertically) light (100:1), as experimentally required. A separate crossed-polarizer arrangement enabled adjustment of the laser intensity. An optical power meter (Coherent Model Powermax PM10) was used to measure the incident laser power at the sample's location. As the red laser beam photothermally heated the GNRs, the increase in average temperature within the polymer was detected by monitoring the perylene fluorescence intensity ratio, as discussed in the previous section.

Fluorescence anisotropy measurement: Fluorescence anisotropy measurements were carried out in a PTI QM40 (Photon Technologies International) spectrofluorometer. The cross-hatched patterned perylene:GNR:PEO mats were fabricated on plastic transparencies and then mounted on a custom-built sample holder. The sample was then irradiated in situ with a 0.1 W/cm^2 808 nm laser, while the emitted perylene fluorescence was measured with right-angle collection. The anisotropy of the sample was recorded as a function of laser irradiation time.

To determine the intrinsic fluorescence anisotropy of a comparable perylene:PEO melt, a concentrated perylene:PEO solution in an open glass cuvette was heated at 40 °C for ~2 days to aid in solvent (water) evaporation, resulting in a well-mixed perylene:PEO solid. The cuvette was mounted on a hotplate, and the anisotropy was measured as a function of temperature (Supporting Information, Figure S3) using the same experimental apparatus as the perylene-based temperature measurement (described above), with linear polarizers introduced along the incident 405 nm laser beam and fluorescence detection paths in order to obtain appropriate polarized excitation and emission beams. The limiting anisotropy values from this approach matched those measured using the commercial spectrofluorometer.

Supporting Information

Supporting Information is available from the Wiley Online Library or from the author.

Acknowledgements

This work was supported by the National Science Foundation (CMMI-0829379, CMMI-1069108, DMR-1056653, and the Research Triangle MRSEC, DMR-1121107), Sigma Xi (GIAR), and the Faculty Research and Professional Development Fund at NC State University. The authors would like to thank Dr. Keith Weninger (NCSU Physics), Dr. Russell Gorga (NCSU Textiles) and Dr. Greg Parsons (NCSU Chemical and Biomolecular Engineering), and the Education and Research Laboratory (NCSU Physics) for use of equipment, Vidya Vishwanath for aid with aligned nanofiber fabrication, Judy Elson for assistance with SEM, and the Advanced Instrumentation Facility (NCSU) for help with TEM.

Received: September 24, 2012
Revised: October 11, 2012

[1] S. Maity, J. R. Bochinski, L. I. Clarke, *Adv. Funct. Mater.* **2012**, *22*, 5259–5270.
[2] S. Maity, L. N. Downen, J. R. Bochinski, L. I. Clarke, *Polymer* **2011**, *52*, 1674–1685.
[3] U. Kreibig, L. Genzel, *Surf. Sci.* **1985**, *156*, 678–700.
[4] C. H. Chou, C. D. Chen, C. R. C. Wang, *J. Phys. Chem. B* **2005**, *109*, 11135–11138.
[5] S. Link, M. A. El-Sayed, *Int. Rev. Phys. Chem.* **2000**, *19*, 409–453.
[6] R. S. Norman, J. W. Stone, A. Gole, C. J. Murphy, T. L. Sabo-Attwood, *Nano Lett.* **2008**, *8*, 302–306.
[7] P. Zijlstra, J. W. M. Chon, M. Gu, *Nature* **2009**, *459*, 410–413.
[8] X. H. Huang, I. H. El-Sayed, W. Qian, M. A. El-Sayed, *J. Am. Chem. Soc.* **2006**, *128*, 2115–2120.
[9] T. B. Huff, L. Tong, Y. Zhao, M. N. Hansen, J. X. Cheng, A. Wei, *Nanomedicine* **2007**, *2*, 125–132.
[10] L. Tong, Y. Zhao, T. B. Huff, M. N. Hansen, A. Wei, J.-X. Cheng, *Adv. Mater.* **2007**, *19*, 3136–3141.
[11] T. Ming, L. Zhao, H. J. Chen, K. C. Woo, J. F. Wang, H. Q. Lin, *Nano Lett.* **2011**, *11*, 2296–2303.
[12] T. Ming, L. Zhao, Z. Yang, H. J. Chen, L. D. Sun, J. F. Wang, C. H. Yan, *Nano Lett.* **2009**, *9*, 3896–3903.
[13] A. Wijaya, S. B. Schaffer, I. G. Pallares, K. Hamad-Schifferli, *ACS Nano* **2008**, *3*, 80–86.
[14] R. Abargues, K. Abderrafi, E. Pedrueza, R. Gradess, J. Marques-Hueso, J. L. Valdes, J. Martinez-Pastor, *New J. Chem.* **2009**, *33*, 1720–1725.

[15] R. D. Deshmukh, Y. Liu, R. J. Composto, *Nano Lett.* **2007**, *7*, 3662–3668.
[16] Y. Dirix, C. Darribere, W. Heffels, C. Bastiaansen, W. Caseri, P. Smith, *Appl. Optics* **1999**, *38*, 6581–6586.
[17] G. Q. Jiang, M. J. A. Hore, S. Gam, R. J. Composto, *ACS Nano* **2012**, *6*, 1578–1588.
[18] C. J. Murphy, C. J. Orendorff, *Adv. Mater.* **2005**, *17*, 2173–2177.
[19] D. Nepal, M. S. Onses, K. Park, M. Jespersen, C. J. Thode, P. F. Nealey, R. A. Vaia, *ACS Nano* **2012**, *6*, 5693–5701.
[20] J. Pérez-Juste, B. Rodríguez-González, P. Mulvaney, L. M. Liz-Marzán, *Adv. Funct. Mater.* **2005**, *15*, 1065–1071.
[21] A. Petukhova, J. Greener, K. Liu, D. Nykypanchuk, R. Nicolay, K. Matyjaszewski, E. Kumacheva, *Small* **2012**, *8*, 731–737.
[22] M. Sethi, G. Joung, M. R. Knecht, *Langmuir* **2009**, *25*, 1572–1581.
[23] Q. Xie, J. Zhou, L. Kang, Q. Zhao, B. Li, Y. H. Wang, R. L. Zong, X. G. Huang, *J. Nanosci. Nanotechnol.* **2010**, *10*, 1829–1833.
[24] K. E. Roskov, K. A. Kozek, W. C. Wu, R. K. Chhetri, A. L. Oldenburg, R. J. Spontak, J. B. Tracy, *Langmuir* **2011**, *27*, 13965–13969.
[25] P. Wang, L. Zhang, Y. Xia, L. Tong, X. Xu, Y. Ying, *Nano Lett.* **2012**, *12*, 3415.
[26] C.-L. Zhang, K.-P. Lv, H.-P. Cong, S.-H. Yu, *Small* **2012**, *8*, 648–653.
[27] G.-M. Kim, A. Wutzler, H.-J. Radusch, G. H. Michler, P. Simon, R. A. Sperling, W. J. Parak, *Chem. Mat.* **2005**, *17*, 4949–4957.
[28] J. H. Lee, J. T. Jang, J. S. Choi, S. H. Moon, S. H. Noh, J. W. Kim, J. G. Kim, I. S. Kim, K. I. Park, J. Cheon, *Nat. Nanotechnol.* **2011**, *6*, 418–422.
[29] C. L. Zhang, K. P. Lv, H. T. Huang, H. P. Cong, S. H. Yu, *Nanoscale* **2012**, *4*, 5348–5355.
[30] C.-L. Zhang, K.-P. Lv, N.-Y. Hu, L. Yu, X.-F. Ren, S.-L. Liu, S.-H. Yu, *Small* **2012**, *8*, 2936–2940.
[31] B. Nikoobakht, M. A. El-Sayed, *Chem. Mat.* **2003**, *15*, 1957–1962.
[32] P. Katta, M. Alessandro, R. D. Ramsier, G. G. Chase, *Nano Lett.* **2004**, *4*, 2215–2218.
[33] E. Zussman, A. Theron, A. L. Yarin, *Appl. Phys. Lett.* **2003**, *82*, 973–975.
[34] S. Link, M. B. Mohamed, M. A. El-Sayed, *J. Phys. Chem. B* **1999**, *103*, 3073–3077.
[35] A. J. Bur, M. G. Vangel, S. Roth, *Appl. Spectrosc.* **2002**, *56*, 174–181.
[36] A. Kawski, *Crit. Rev. Anal. Chem.* **1993**, *23*, 459–529.
[37] J. R. Lakowicz, *Principles of Fluorescence Spectroscopy*3rd ed., Springer, **2006**.
[38] E. Engel, K. Schmidt, D. Beljonne, J. L. Bredas, J. Assa, H. Frob, K. Leo, M. Hoffmann, *Phys. Rev. B* **2006**, *73*, 9.
[39] J. R. Lakowicz, J. R. Knutson, *Biochemistry* **1980**, *19*, 905–911.
[40] D. W. Piston, T. Bilash, E. Gratton, *J. Phys. Chem.* **1989**, *93*, 3963–3967.
[41] S. D. McCullen, K. L. Stano, D. R. Stevens, W. A. Roberts, N. A. Monteiro-Riviere, L. I. Clarke, R. E. Gorga, *J. Appl. Polym. Sci.* **2007**, *105*, 1668–1678.
[42] S. D. McCullen, D. R. Stevens, W. A. Roberts, S. S. Ojha, L. I. Clarke, R. E. Gorga, *Macromolecules* **2007**, *40*, 997–1003.
[43] S. S. Ojha, D. R. Stevens, T. J. Hoffman, K. Stano, R. Klossner, M. C. Scott, W. Krause, L. I. Clarke, R. E. Gorga, *Biomacromolecules* **2008**, *9*, 2523–2529.
[44] S. S. Ojha, D. R. Stevens, K. Stano, T. Hoffman, L. I. Clarke, R. E. Gorga, *Macromolecules* **2008**, *41*, 2509–2513.

Particle
Submitted to & Particle Systems Characterization

Supporting Information

for *Part. Part. Sys. Charact.*, DOI: 10.1002/ppsc. 201200084

Anisotropic Thermal Processing of Polymer Nanocomposites via the Photothermal Effect of Gold Nanorods

*Somsubhra Maity, Krystian Kozek, Wei-Chen Wu, Joseph Tracy, Jason Bochinski, and Laura Clarke**

To validate the orientation of the gold nanorods (GNRs) within the vertically aligned nanofibers, the linear polarizer was fixed and the sample itself was rotated from 0° - 90° in increments of 15° (Figure S1a). An identical experiment was performed on uniaxially-aligned fibers doped solely with spherical gold nanoparticles to demonstrate the angle-independent extinction of the nanospheres (Figure S1b).

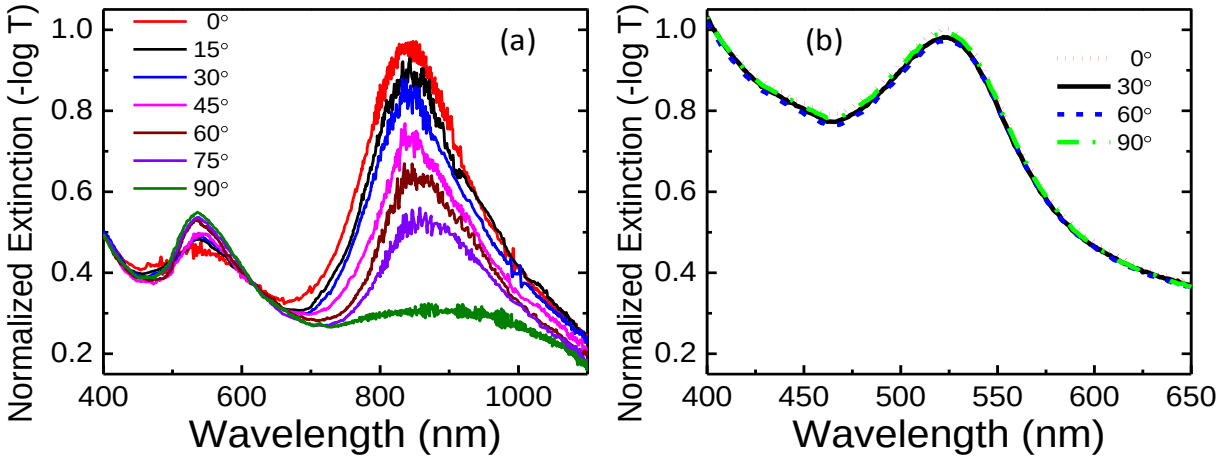

Figure S1. (a) Normalized extinction spectra of a uniaxially-aligned PEO:GNR nanofibrous mat at varying angles between the fiber orientation direction and the incident light linear polarization direction from 0° to 90° where the sample was rotated in increments of 15°. The feature at ~535 nm is due to both the polarization-dependent TSPR of GNRs and the polarization-insensitive SPR from the small population of spherical nanoparticles. The peak at ~850 nm due to the LSPR of GNRs shows a reduction in amplitude as the relative angle changes from 0° to 90°. (b) An identical experiment with uniaxially-aligned PEO nanofibers doped with spherical gold nanoparticles (diameter = 20-30 nm). The sample does not display any angle-dependent extinction as it is rotated from 0° to 90°, demonstrating that the angle-specific absorption in PEO:GNR nanofibers from part (a) is entirely due to the GNRs. A background subtraction equal to the extinction of a similarly-thick, PEO-only uniaxially-aligned fiber sample has been applied to each angle.

The fluorophore perylene acts as a local temperature sensor when embedded within polymer composite material; the contribution from many fluorophores gives an average temperature of the sample. The ratio of fluorescence intensity measured at two distinct wavelengths (trough and peak) for a given polymeric system provides a quasi-linear temperature relationship.

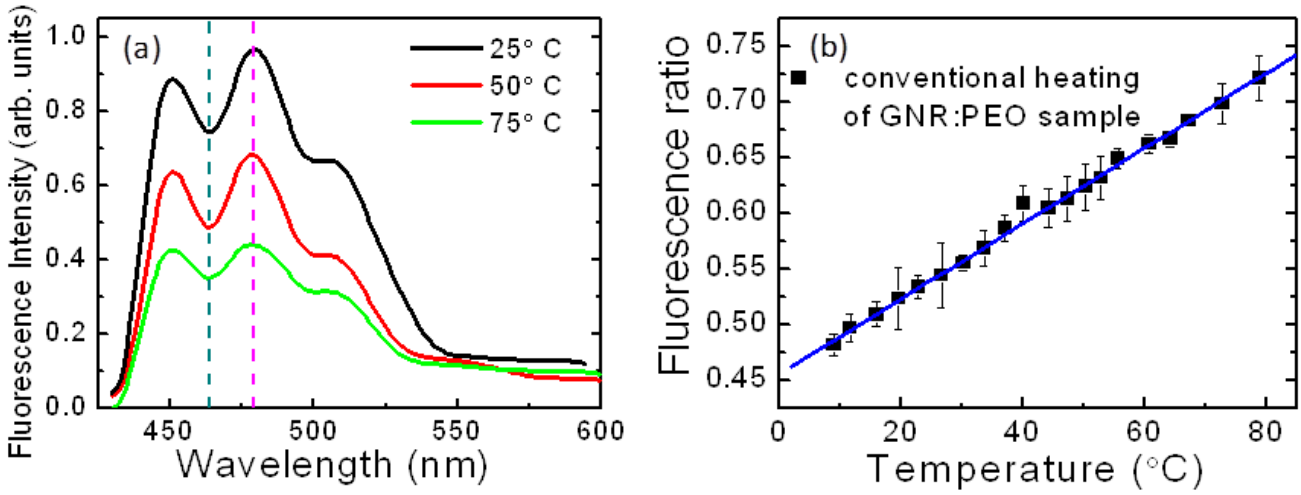

Figure S2. (a) Fluorescence intensity of perylene embedded in a PEO matrix changes with temperature. The ratio of the measured perylene emission intensities at 465 nm to that at 479 nm (dotted lines) increases with sample temperature. (b) Measured calibration curve of the fluorescence ratio when the perylene-polymer composite is heated conventionally.

Figure S3 depicts the change in the *r*-factor of the perylene:PEO composite as it transforms from a solid to a melt phase.

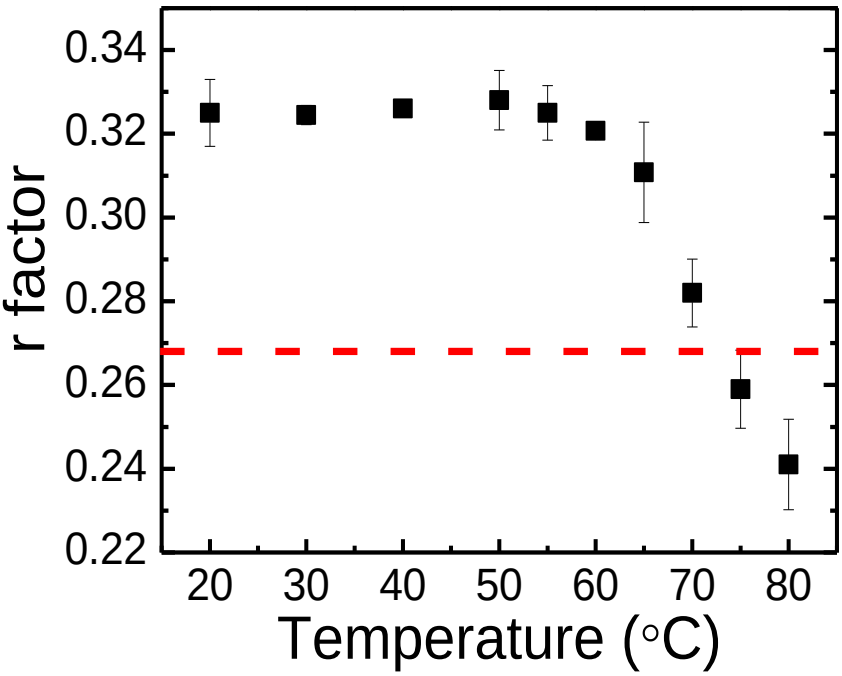

Figure S3. The change in the anisotropy of perylene within a PEO solid as the temperature is increased. The r-factor value remains approximately constant at 0.325 up until a temperature of 60 °C, above which it decreases, reaching a value of ~0.24 at 80 °C. The dotted line indicates the anisotropy value obtained during photothermal treatment of aligned GNR:PEO nanofibers, suggesting an average temperature of ~70 °C was locally realized.